Role of final state interactions in quasielastic ^{56}Fe(e, e') reactions at large $|\vec{q}|$

C. R. Chinn

Department of Physics and Astronomy, Vanderbilt University, Nashville, Tennessee 37235

(Received 17 October 1994)

A relativistic finite nucleus calculation using a Dirac optical potential is used to investigate the importance of final state interactions (FSI) at large momentum transfers in inclusive quasielastic electronuclear reactions. The optical potential is derived from first-order multiple scattering theory and then is used to calculate the FSI in a nonspectral Green's function doorway approach. At intermediate momentum transfers excellent predictions of the quasielastic ^{56}Fe(e, e') experimental data for the longitudinal response function are obtained. In comparisons with recent measurements at $|\vec{q}| = 1.14$ GeV/c the theoretical calculations of R_L give good agreement for the quasielastic peak shape and amplitude, but place the position of the peak at an energy transfer of about 40 MeV higher than the data.

I. INTRODUCTION

There has been a recent interest in inclusive quasielastic electronuclear reactions at large momentum transfers ($|\vec{q}| \gtrsim 1$ GeV/c), especially with the upcoming programs planned at CEBAF. Along with recent measurements [1] there has been some theoretical work investigating the physical role of relativity and final state interactions (FSI) in such reactions [2,3]. From these studies it has been noted that a full finite nucleus calculation would be helpful in discerning the various physical contributions. This paper attempts to address that need.

In the simple relativistic Fermi gas calculation of Ref. [2] the implications were that the role of FSI at $|\vec{q}| \gtrsim 1$ GeV/c appeared to be greatly reduced, especially since the use of a real energy-independent potential to model the FSI caused the predicted position of the quasielastic peak to move significantly away from the data. The use of a Fermi gas model may be misleading, however, since the recoil effects will be misrepresented which may affect the calculated position of the quasielastic peak. A finite nucleus model should be more appropriate. In Ref. [3] an energy-dependent real potential was introduced to give the FSI, and the conclusion from this study is that the FSI remain important at large $|\vec{q}|$, and that the energy dependence is required to enable one to predict the peak position correctly. In that work the imaginary part of the optical potential is neglected. From optical model studies of elastic nucleon-nucleus scattering and from multiple scattering theory there is known to be a strong energy dependence in the optical potentials. To delete the imaginary part of an energy-dependent potential is to break the unitarity constraint and thus incorrectly represent the reactive content of the optical potential. For a more physical representation, the full complex energy-dependent optical potential should be included in a consistent manner. The importance of such considerations was discussed in detail in Ref. [4].

In this paper two complex energy-dependent Dirac optical potentials derived from multiple scattering are used in a relativistic finite-nucleus calculation to calculate the separated response functions for inclusive quasielastic (e, e') scattering from ^{56}Fe. In these calculations Dirac dynamical effects resulting from couplings to negative energy states, which were shown in Ref. [4] to be important, are included. In Sec. II a theoretical discussion of the model and the calculation is presented. The results and the comparison with the experimental measurements, along with a discussion of current conservation issues, are presented in Sec. III followed by a conclusion.

II. THEORETICAL DISCUSSION

Although the main mechanism in quasielastic reactions is assumed to be the knockout of a single nucleon, in inclusive reactions all possible final states are included in the experimental measurements. The optical potential implies the existence of other final states besides the knockout channel within the imaginary part. For this reason to include all of the possible final states implied by an optical potential the nonspectral Green's function doorway approach [5], which is discussed more fully in Ref. [4], is used. The longitudinal and transverse response functions within the one-photon-exchange approximation are given by

$$R_L(\vec{q}, \omega) = W^{00}(\vec{q}, \omega),$$
$$R_T(\vec{q}, \omega) = W^{11}(\vec{q}, \omega) + W^{22}(\vec{q}, \omega), \qquad (2.1)$$

where

$$W^{\mu\nu} = \overline{\sum_i} \sum_f \langle i | \hat{J}^\mu(q)^\dagger | f \rangle \delta(E_i + \omega - E_f) \langle f | \hat{J}^\nu(q) | i \rangle. \qquad (2.2)$$

Here $|i\rangle$ represents the initial nuclear many-body state, while the sum over $|f\rangle$ corresponds to all final states of

the full hadronic many-body assembly. $\hat{J}^\mu(q)$ is the electromagnetic nuclear current operator, and the $\overline{\sum_i}$ denotes an average over the initial states.

One would like to perform an explicit sum over the complete set of complex inelastic reaction channels in the final state, but in practice such a many-body calculation is prohibitively difficult. Therefore a nonspectral approach is used where the sum over all of the final states within a particular space is implicitly performed, by considering the full A-body Green's function.

Suppressing the discrete state contribution, Eq. (2.2) can be rewritten in terms of the forward virtual Compton amplitude:

$$W^{\mu\nu}(\vec{q},\omega) = -\frac{1}{\pi} Im T^{\mu\nu}(\vec{q},\omega),   (2.3)$$

where

$$T^{\mu\nu}(\vec{q},\omega) = \overline{\sum_i}\langle i|\hat{J}^\mu(q)^\dagger \hat{G}(\omega + E_i)\hat{J}^\nu(q)|i\rangle.   (2.4)$$

Here $\hat{G}$ is the full many-body propagator for the A-nucleon system. If $\hat{J}^\mu$ is assumed to be a one-body operator, it can be shown [4] that within this one-body space $\hat{G}$ reduces to the optical model Green's function. By using the optical model Green's function in a nonspectral form, then a consistent unitary representation of the reactive content of the final state interactions is maintained [4]. If one assumes that each knockout channel is represented by the same optical model potential, then the following substitution can be made:

$$\hat{G} \approx \hat{G}_{\rm opt} = \hat{G}_0 + \hat{G}_0 \hat{U}_{\rm opt} \hat{G}_{\rm opt}.   (2.5)$$

$\hat{G}_{\rm opt}$ corresponds to the use of an optical model potential to represent the final state interactions between the ejected nucleon and the residual nucleus. $\hat{G}_0$ is the free propagator for a nucleon within the nuclear medium.

To reduce the calculation to the plane wave approximation (PWA), $\hat{U}_{\rm opt}$ is set to zero or equivalently

$$\hat{G} \approx \hat{G}_0,   (2.6)$$

which leads to Eq. (2.2), where only final plane wave states for the ejected nucleon are considered.

The calculations are performed in a fully-off-shell momentum space representation:

$$T^{\mu\nu}(\vec{q},\omega) = \overline{\sum_i}\int \frac{d^3\vec{p}\,d^3\vec{p}'}{2\pi^3}\langle i|\vec{p} - \vec{q}\rangle\, J^\mu(-q)\, G_{\rm opt}(\vec{p},\vec{p}';E)$$
$$\times J^\nu(p')\,\langle \vec{p}' - \vec{q}\,|i\rangle .   (2.7)$$

Here $G_{\rm opt}(\vec{p},\vec{p}';E)$ is calculated from the fully off-shell relativistic optical potential as derived from multiple scattering theory. The optical model Green's function is calculated as the solution of the Lippmann-Schwinger equation in momentum space to give the fully-off-shell nucleon-nucleus T matrix. The equations are solved in partial wave form so as to include the spin-orbit contributions in a convenient way:

$$G_{\rm opt}(\vec{p},\vec{p}';E)= G_0(p;E)\,\delta^{(3)}(\vec{p}-\vec{p}')$$
$$+G_0(p;E)\int V_{\rm opt}(\vec{p},\vec{p}'')G_{\rm opt}(\vec{p}'',\vec{p}';E)d^3\vec{p}''$$
$$= G_0(p;E)\,\delta^{(3)}(\vec{p}-\vec{p}') + G_0(p;E)$$
$$\times T_{\rm opt}(\vec{p},\vec{p}';E)\,G_0(p';E),   (2.8)$$

$$T_{\rm opt}(\vec{p},\vec{p}';E) = V_{\rm opt}(\vec{p},\vec{p}') +\int d^3\vec{p}''\, V_{\rm opt}(\vec{p},\vec{p}'')\, G_0(p'';E)$$
$$\times T_{\rm opt}(\vec{p}'',\vec{p}';E).   (2.9)$$

In the above equation the free Dirac propagator can be separated into a positive-energy projecting part and a negative-energy projecting part, so that contributions to Eq. (2.7) involve coupling to the negative-energy Dirac sea. It has been shown that such effects can play a major role in the calculated response functions [4,6–8].

The negative-energy contributions referred to above require some discussion, since these contributions differ from those that arise from relativistic RPA calculations [9]. The negative-energy contributions in relativistic RPA arise from the summation of ring diagrams through a one-particle one-hole subspace. This comes about due to the approximation of the single particle propagator with a mean field propagator, which includes the Hartree mean field and RPA correlations. In the model presented in this paper the single particle propagator is approximated by the optical model Green's function. As shown in Ref. [10] contributions derived from an optical potential in this case are equivalent to n-particle n-hole contributions, where $n \geq 2$. RPA effects are not included in this paper, and the negative-energy contributions implied in Eqs. (2.8) and (2.9) arise from couplings to the reactive content of the optical potential and are outside of the pure one-particle one-hole picture.

In the PWA and FSI calculations a single particle description is used. Bound state wave functions are taken from a Dirac-Hartree calculation [11] and are represented in Dirac four-spinor form. Since the Dirac-Hartree calculation performed in Ref. [11] assumes spherical symmetry and ^{56}Fe is not a doubly magic closed shell nuclei, approximations are used to represent the valence nucleons. In this case the valence shell is represented as a closed shell, but with fractional occupation numbers to give 26 protons and 30 neutrons. The current operators are treated in relativistic form, and no nonrelativistic reduction is performed.

The analysis presented in this paper will be performed for both (a) the relativistic plane wave approximation and (b) with the Green's function doorway approach to include the FSI. The form of the electromagnetic nucleon current inside of the nucleus is unknown, hence two different functional forms of the free electromagnetic current operator are used:

$$\hat{J}^\mu_{cc2} = F_1(q^2)\gamma^\mu + i\frac{F_2(q^2)}{2m}\sigma^{\mu\nu}q_\nu,$$

and   (2.10)

$$\hat{J}^\mu_{cc1} = G_m(q^2)\gamma^\mu - \frac{F_2(q^2)}{2m}\bar{\mathcal{K}}^\mu$$
$$= F_1(q^2)\gamma^\mu + i\frac{F_2(q^2)}{2m}\sigma^{\mu\nu}\bar{q}_\nu,$$

where $G_m = F_1 + F_2$ is the familiar Sachs magnetic form factor and $\mathcal{K} \equiv k + k'$. The bars over $\bar{\mathcal{K}}$ and $\bar{q}$ indicate that k and k' are fixed to the on-shell values, e.g., $\bar{k}^o \equiv \pm\sqrt{\bar{k}^2 + m^2}$, where the sign is dependent upon the $(\pm)$ energy character of the Dirac spinor. The definitions of $\widehat{J}_{cc2}$ and $\widehat{J}_{cc1}$ correspond to the $cc2$ and $cc1$ operators defined in Ref. [12]. These two operators are identical on-shell and hence give the same free nucleon electromagnetic representations. In the off-shell case where one scatters from bound nucleons or when one includes FSI, these operators give differing results. The most general form of the current operator contains 12 independent terms, in which only two independent terms survive in the on-shell limit. To be able to construct the complete operator with the accompanying form factors one would require a reliable off-shell nucleon structure model, for example, a QCD-based model. Hence the calculated differences between the $cc1$ and $cc2$ operators can only be understood in terms of the underlying nucleon structure. For a detailed analysis of the effects and uncertainties represented by these two operators, please see Refs. [7,13,14].

Current conservation is imposed by means of the standard replacement of $\widehat{q} \cdot \vec{J}$ by $q_o J^o / |\vec{q}|$. In general the current is not conserved by these two operators, since there typically is not a consistent Hamiltonian treatment of the initial state, the final state, and the electromagnetic current interactions. The form factors used in this paper are taken from Ref. [15]. An analysis of current conservation is presented at the end of the following section.

Two relativistic complex optical potentials derived from multiple scattering theory are used to represent the FSI. In this case nucleon-nucleon $[NN]$ t matrices are folded with local densities in the optimum factorization approximation [16] to give the optical potential. The negative-energy part of the optical potential is constructed using an approximate approach [17]. For one optical potential the NN t matrices are calculated from the fully-off-shell full Bonn potential [18], which include the effects of relativistic kinematics, retarded meson propagators as given by time-ordered perturbation theory, and crossed and iterative meson exchanges with NN, $N\Delta$, and $\Delta\Delta$ intermediate states. For ejectile energies greater than 300 MeV, an extension of the Bonn meson exchange interaction above pion production threshold is used [19]. The second optical potential uses the NN interaction of Ref. [20]. The proton densities are taken from electron scattering measurements [21], while the neutron densities are those calculated from the Hartree-Fock-Bogolyubov calculation of Ref. [22]. In calculations of elastic nucleon-nucleus scattering, the use of the Bonn potential tends to give a better representation of the data than the Franey-Love amplitudes, probably due to the superior off-shell behavior of the Bonn potential.

In this paper the nonrelativistic calculations of FSI are constructed from the relativistic calculations with the exception that all of the negative energy contributions which result from the Dirac dynamics are neglected. This includes those negative energy contributions that arise from the construction of $\widehat{U}_{\rm opt}$ and in the calculation of $\widehat{G}_{\rm opt}$. This is the manner in which the nonrelativistic cal-

culation is calculated here, where relativistic kinematics are maintained.

III. RESULTS AND COMPARISONS WITH THE DATA

To gauge the accuracy of the theoretical model, comparisons with quasielastic ^{56}Fe(e, e') data are made at $|\vec{q}| = 410$ and 550 MeV/c. These comparisons are made both with nonrelativistic FSI and with relativistic FSI including Dirac dynamical degrees of freedom. The PWA results with no FSI $(V_{\rm opt} = 0)$, and the nonrelativistic FSI calculations are shown in Figs. 1 and 2 for $|\vec{q}| = 410$ and 550 MeV/c, respectively. The PWA calculation places the peak position for R_L in the upper panels at an energy transfer of about $15 - 25$ MeV larger than the experimental data. Note that these data do not include any Coulomb distortion corrections, which may shift the experimental result. After including the nonrelativistic FSI, one can see the peak position is much better represented with the error in R_L being negligible.

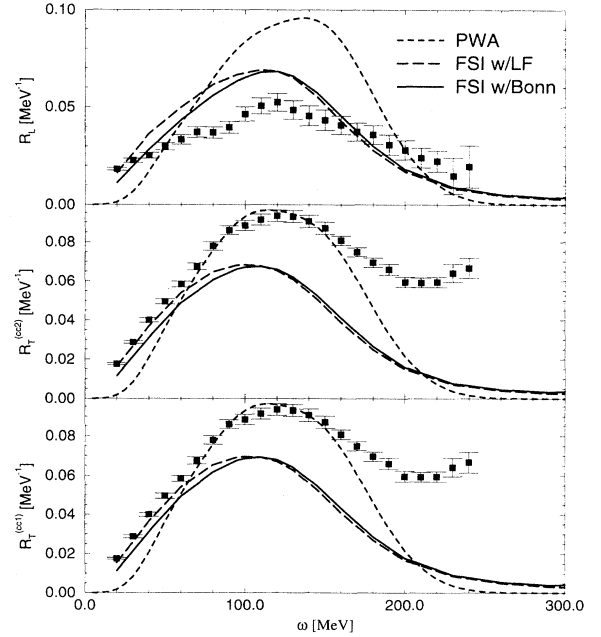The use of the Bonn potential in the solid curve gives a slightly different result than the long-dashed curve,

FIG. 1. The inclusive quasielastic separated response functions are shown for scattering from ^{56}Fe at $|\vec{q}| = 410$ MeV/c. The longitudinal response is shown in the upper panel. The transverse response function calculated using the $cc2$ (Dirac) and the $cc1$ electromagnetic nucleon current operators is shown in the middle and lower panels, respectively. The short-dashed curves represent the PWA calculation. The solid and long-dashed curves correspond to the nonrelativistic FSI calculation using optical potentials calculated with the full Bonn potential and Franey-Love amplitudes, respectively. The data do not include any Coulomb distortion corrections and are from Ref. [23].
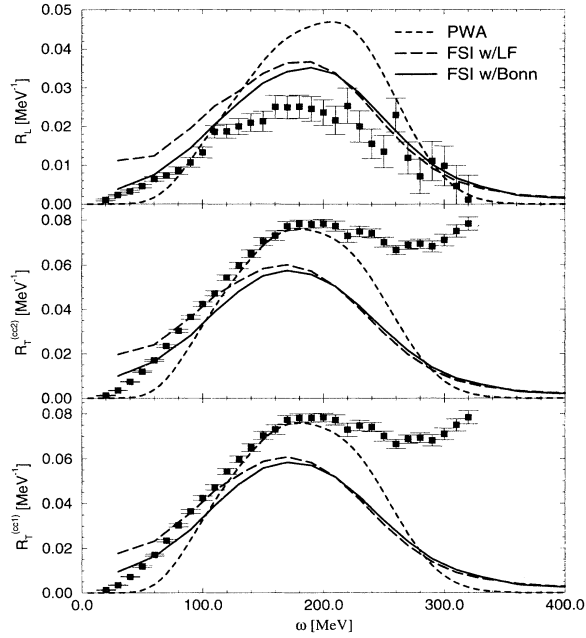
FIG. 2. The same as Fig. 1, except at $|\vec{q}| = 550$ MeV/c.

FIG. 3. The same as Fig. 1, except the FSI are calculated using the relativistic model including Dirac dynamical effects.

which uses the Franey-Love amplitudes. In this case the Bonn potential gives a slightly better representation of the data.

In the middle and lower panels of Figs. 1 and 2 the transverse response is calculated. In this case there are two possible predictions for the same data due to the ambiguity about the $\hat{J}_{cc1}$ and $\hat{J}_{cc2}$ current operators in Eq. (2.10). These two operators give formally identical longitudinal results, but differ in the transverse channel. For the nonrelativistic case this difference is very small. Since the Δ resonance is not included in this calculation the comparisons with the data can only be made qualitatively. From the tail of the Δ resonance in the curves, it appears that the nonrelativistic FSI predictions will underestimate the data.

The relativistic FSI results for $|\vec{q}| = 410$ and 550 MeV/c are shown in Figs. 3 and 4, respectively. Here the predictions of R_L are very close, where the Bonn potential gives a slightly larger R_L than the Franey-Love amplitudes. The peak positions are accurate and the overall peak is well represented.

For the transverse case the $cc2$ or Dirac current results shown in the middle panels greatly underestimate the data, while the $cc1$ current results are very close to the data, although the inclusion of the Δ-resonance degrees of freedom may easily alter this agreement. The large differences between Dirac current and $cc1$ current predictions for the relativistic transverse response calculation are related to the definition of the $cc1$ current operator. The difference between the two current operators used here is that the $cc1$ operator uses $\bar{q}_\mu$ or $\bar{\omega}$ and thus requires the on-shell energies to be used. For the negative-energy states these on-shell energies are
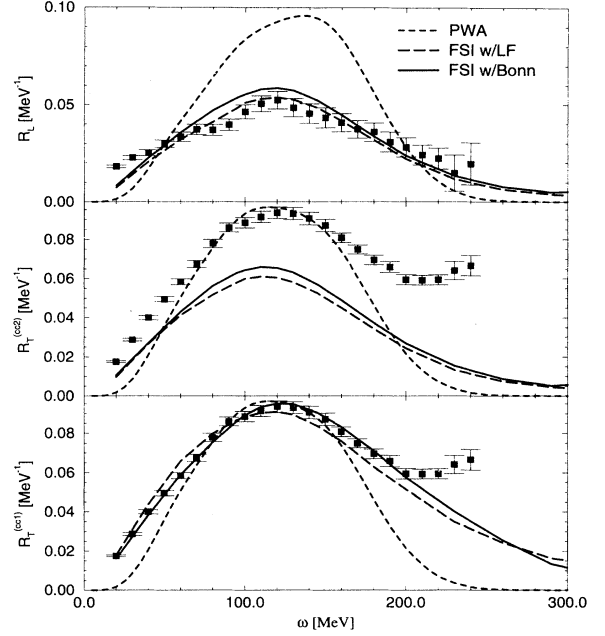
$\bar{k}^0 = -\sqrt{\vec{k}^2 + m^2}$. Hence the off-shell difference between the Dirac current and the $cc1$ current become much more exagerated for the negative-energy states, since here $\bar{\omega}$ becomes very different from ω.

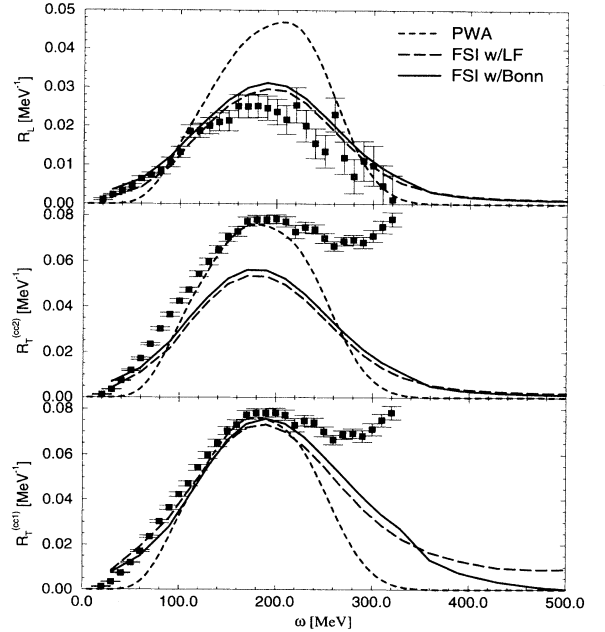From the R_L comparisons the relativistic dynamical effects are very important in providing good theoretical

FIG. 4. The same as Fig. 1, except at $|\vec{q}| = 550$ MeV/c and the FSI are calculated using the relativistic model including Dirac dynamical effects.

predictions of the data at these intermediate momentum transfers. For greater momentum transfers one would expect that relativistic effects to be an important and necessary ingredient for any accurate theoretical description of the data.

The quasielastic ^{56}Fe(e, e') results for a momentum transfer of $|\vec{q}| = 1.14$ GeV/c are shown in Figs. 5 and 6 using nonrelativistic and relativistic FSI, respectively. Here the PWA result for R_L places the peak positions at an energy transfer which is about 55 MeV greater than the peak in the data. With nonrelativistic FSI, the peak position is closer to the data but still about $30-45$ MeV too high. With relativistic FSI in Fig. 6 the Dirac dynamical effects move the predicted peak further away to be about $40-50$ MeV higher in ω than the data. In this case the shapes of the peak in R_L are well represented, although a bit too wide, while the peak position is not as accurately placed. The relativistic FSI calculation gives a smaller amplitude peak than the nonrelativistic FSI calculation and is closer to the circled data, which take into account in an approximate fashion the Coulomb distortions. It is interesting to note that the relatively large errors are not truly able to discern clearly between the relativistic and nonrelativistic FSI calculations. The Coulomb corrected data appear to favor the need for relativistic FSI. The predicted peak position in Fig. 6 is actually closer than the most sophisticated results of Ref. [3], which places the peak position at an ω of about 85 MeV higher than the data. It is clear from Fig. 6 that FSI are very important effects at even this high momentum transfer, although one would like to obtain a more accurate prediction of the peak position.
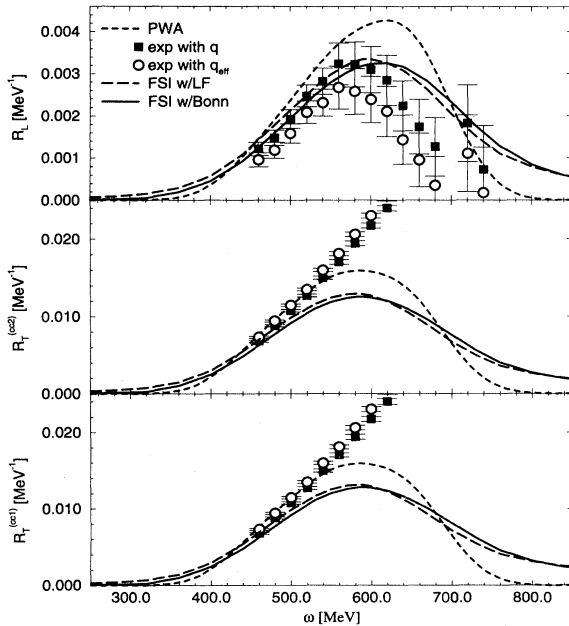

FIG. 6. The same as Fig. 1, except at $|\vec{q}| = 1.14$ GeV/c and the FSI are calculated using the relativistic model including Dirac dynamical effects and the data are from Ref. [1]. The data represented by the circles account for Coulomb distortion effects by using an effective q, while the squares omit this correction.
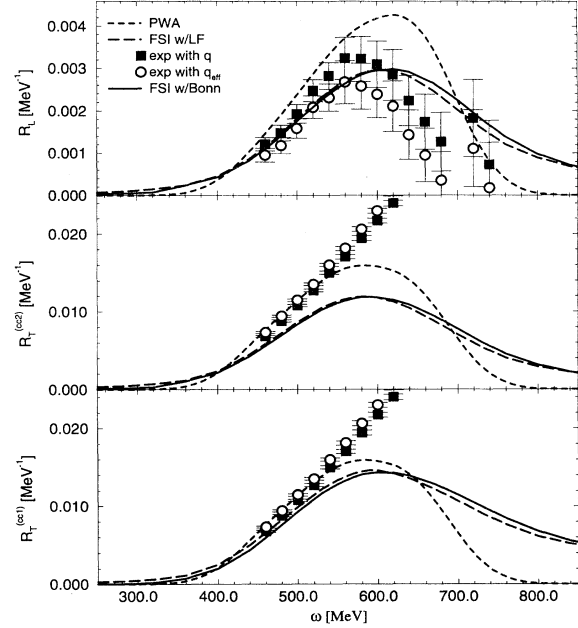

FIG. 5. The same as Fig. 1, except at $|\vec{q}| = 1.14$ GeV/c and the data are from Ref. [1]. The data represented by the circles account for Coulomb distortion effects by using an effective q, while the squares omit this correction.

In some sense in Fig. 6, 40 MeV does not seem like a large number, but on the scale of Figs. 3 and 4 this value becomes significant. The incorrect peak position seen in Fig. 6 cannot be interpreted in terms of an average binding energy shift, since this would also affect the intermediate energy range results by the same amount, where the peak positions are accurately reproduced. The shift in the peak position must arise from a dynamical effect. There are a number of possible candidates for such an effect, such as the restoration of current conservation, meson exchange effects, ambiguities in the off-shell structure of the electromagnetic current, FSI effects not included in an optical model description, better treatment of the Coulomb distortions, or even the need for a fully causal or Lorentz invariant description. With the advent CEBAF, comparisons with other more accurate experimental results, especially in the $(e, e'p)$ case, may prove to be very enlightening.

Although the model used here provides a realistic formalism for including FSI, there remains the question as to whether the lack of current conservation would alter any of the results of this calculation. As a measure of the violation of current conservation the longitudinal response can also be calculated using the third component of the current operator instead of the time component. In this case by using J^3 instead of J^0 the longitudinal response can be calculated as $R_L^{(3)}(\vec{q}, \omega) = \left(\dfrac{|\vec{q}|}{\omega}\right)^2 W^{33}(\vec{q}, \omega)$. The results comparing the two ver-

sions of the longitudinal response are shown in Figs. 7 and 8 for $|\vec{q}| = 550$ and 1140 MeV/c, respectively. In the upper panels of these two figures the plane wave approximation calculations are shown. In this case the two current operators used give identical expressions for the zeroth component, but give different z-component expressions. The calculations for the two current operators in the PWA result in almost identical results. For $R_L^{(3)}$ at $|\vec{q}| = 550$ MeV/c the current conservation violation in the PWA appears to be rather large. This can be understood in the sense that the initial state Hamiltonian involves the Dirac Hartree potential, while the final state is the free Hamiltonian and thus the current conservation violation should be large. It is interesting to note that this violation is reduced greatly at $|\vec{q}| = 1.14$ GeV/c.

In the lower panels of Figs. 7 and 8 the results with the current conservation test are shown where both relativistic and nonrelativistic FSI are included using the Bonn potential and the standard Dirac form of the current operator. In Fig. 7 in the lower panel the relativistic results using both the zeroth and the third component of the current operator are close together, less than the error in the data, indicating the violation of current conservation is probably negligible. The difference between the two nonrelativistic results is curiously larger than that observed for the relativistic comparison. For energy transfer, $\omega < 100$ MeV the violation of current conservation grows dramatically. This is also seen in the results at

FIG. 8. The same as Fig. 7, except for $|\vec{q}| = 1.14$ GeV/c.

$|\vec{q}| = 410$ MeV/c. This indicates that the Hamiltonian descriptions of the initial and final states used here begin to differ significantly for these energies. In Fig. 8 a simlar result is found, although the differences are a little smaller than those observed at $|\vec{q}| = 550$ MeV/c. The result is that there are apparent violations of current conservation, but it appears that these violations are probably smaller than the uncertainty in the data and can be neglected. At some time in the future this issue needs to be studied thoroughly.

IV. CONCLUSION

The longitudinal and transverse response functions for the inclusive quasielastic electronuclear scattering reaction from ^{56}Fe are calculated using a relativistic finite nucleus model with FSI and Dirac dynamical degrees of freedom. FSI are included using the optical model Green's function doorway formalism, which for the case of a one-body electromagnetic current operator provides a physical description of the final states resulting from the reactive content implied by the imaginary part of the optical potential. The optical model Green's function is calculated in a fully-off-shell momentum space calculation using optical potentials derived from first-order multiple scattering theory using two different nucleon-nucleon interactions.

It is found that at intermediate momentum transfers of 410 and 550 MeV/c, the relativistic FSI calculation gives a very good theoretical description of the data, reproducing well the position, shape, and amplitude of the quasielastic peak. At $|\vec{q}| = 1.14$ GeV/c comparisons with recent data find that the shape and amplitude of the peak are well produced, but that the peak is placed at an energy transfer of about 40 MeV higher than the experimental result. The source of this discrepancy is not clear and may provide a motivation for future investigations.

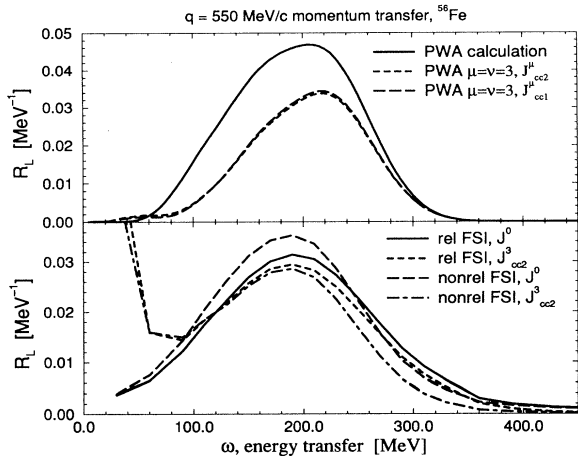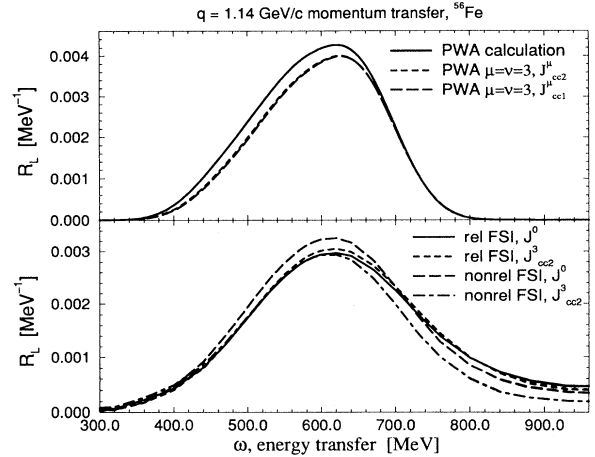An analysis of the effects of current conservation viola-

FIG. 7. The longitudinal response function is calculated by using both the zeroth and third components of the current operator for $|\vec{q}| = 550$ MeV/c. The upper panel shows the PWA result where the solid line uses the zeroth component, while the short-dashed and long-dashed curves use the third component of the current, using the $cc2$ and $cc1$ versions of the current operator, respectively. In the lower panel the results which include FSI and use the $cc2$ version of the current operator are shown. The solid and short-dashed curves include relativistic FSI calculated with the zeroth and third components of the current operator, respectively. The long-dashed and dot-dashed curves include nonrelativistic FSI calculated with the zeroth and third components of the current operator, respectively.

tions indicates that for the energy transfers of interest in this paper these violations are probably not important.

ACKNOWLEDGMENTS

[1] J. P. Chen et al., Phys. Rev. Lett. **66**, 1283 (1991).
[2] M. R. Frank, Phys. Rev. C **49**, 555 (1994).
[3] H. Kim, C. J. Horowitz, and M. R. Frank, Phys. Rev. C **51**, 792 (1995).
[4] C. R. Chinn, A. Picklesimer, and J. W. Van Orden, Phys. Rev. C **40**, 790 (1989).
[5] Y. Horikawa, F. Lenz, and N. C. Mukhopadhyay, Phys. Rev. C **22**, 1680 (1980).
[6] C. R. Chinn, A. Picklesimer, and J. W. Van Orden, Phys. Rev. C **40**, 1159 (1989).
[7] C. R. Chinn and A. Picklesimer, Nuovo Cimento **105A**, 1149 (1992).
[8] C. R. Chinn, Phys. Rev. C **50**, 1509 (1994).
[9] See, for example, S. A. Chin, Ann. Phys. (N.Y.) **108**, 301 (1977); C. J. Horowitz and J. Piekarewicz, Nucl. Phys. **A511**, 461 (1990); J. R. Shepard, E. Rost, and J. A. McNeil, Phys. Rev. C **40**, 2320 (1989).
[10] See, for example, R. D. Smith and J. Wambach, Phys. Rev. C **38**, 100 (1988); G. Co', K. F. Quader, R. D. Smith, and J. Wambach, Nucl. Phys. **A485**, 61 (1988); S. Fantoni and V. R. Pandharipande, ibid. **A473**, 234 (1987).
[11] C. J. Horowitz and B. D. Serot, Nucl. Phys. **A368**, 503 (1981).
[12] T. de Forest, Nucl. Phys. **A392**, 232 (1983).
[13] H. W. L. Naus and J. H. Koch, Phys. Rev. C **36**, 2459 (1987).
[14] P. C. Tiemeijer and J. A. Tjon, Phys. Rev. C **42**, 599 (1990).
[15] M. Gari and W. Krumpelmann, Phys. Lett. B **173**, 10 (1986).
[16] A. Picklesimer, P. C. Tandy, R. M. Thaler, and D. H. Wolfe, Phys. Rev. C **30**, 1861 (1984).
[17] M. V. Hynes, A. Picklesimer, P. C. Tandy, and R. M. Thaler, Phys. Rev. C **31**, 1438 (1985).
[18] R. Machleidt, K. Holinde, and Ch. Elster, Phys. Rep. **149**, 1 (1987).
[19] Ch. Elster and P. C. Tandy, Phys. Rev. C **40**, 881 (1989).
[20] M. A. Franey and W. G. Love, Phys. Rev. C **31**, 488 (1985).
[21] H. D. Wohlfahrt, Habilitationsschrift, University of Mainz, 1976, unpublished.
[22] J.-F. Berger, M. Girod, and D. Gogny, Nucl. Phys. **A502**, 85c (1989).
[23] Z. E. Meziani et al., Phys. Rev. Lett. **52**, 2130 (1984).